JACC: CARDIOVASCULAR IMAGING VOL. 7, NO. 3, 2014

ISSN 1936-878X/$36.00
PUBLISHED BY ELSEVIER INC. http://dx.doi.org/10.1016/j.jcmg.2013.06.008

Dynamic Myocardial CT Perfusion Imaging for Evaluation of Myocardial Ischemia as Determined by MR Imaging

Fabian Bamberg, MD, MPH,*† Roy P. Marcus, BS,* Alexander Becker, MD,‡ Kristof Hildebrandt, BS,* Kerstin Bauner, MD,* Florian Schwarz, MD,*† Martin Greif, MD,‡ Franz von Ziegler, MD,‡ Bernhard Bischoff, MD,* Hans-Christoph Becker, MD,*† Thorsten R. Johnson, MD,* Maximilian F. Reiser, MD,*† Konstantin Nikolaou, MD,*† Daniel Theisen, MD*†

Munich, Germany

OBJECTIVES The aim of this study was to determine the feasibility of computed tomography (CT)-based dynamic myocardial perfusion imaging for the assessment of myocardial ischemia and infarction compared with cardiac magnetic resonance (CMR).

BACKGROUND Sequential myocardial CT perfusion imaging has emerged as a novel imaging technique for the assessment of myocardial hypoperfusion.

METHODS We prospectively enrolled subjects with known coronary artery disease who underwent adenosine-mediated stress dynamic dual-source CT (100 kV, 320 mAs/rot) and CMR (3-T). Estimated myocardial blood flow (eMBF) and estimated myocardial blood volume (eMBV) were derived from CT images, using a model-based parametric deconvolution technique. The values were independently related to perfusion defects (ischemic and/or infarcted myocardial segments) as visually assessed during rest/stress and late gadolinium enhancement CMR. Conventional measures of diagnostic accuracy and differences in eMBF/eMBV were determined.

RESULTS Of 38 enrolled subjects, 31 (mean age 70.4 ± 9.3 years; 77% men) completed both CT and CMR protocols. The prevalence of ischemic and infarcted myocardial segments detected by CMR was moderate (11.6%, n = 56 and 12.6%, n = 61, respectively, of 484 analyzed segments, with 8.4% being transmural). The diagnostic accuracy of CT for the detection of any perfusion defect was good (eMBF threshold, 88 ml/mg/min; sensitivity, 77.8% [95% confidence interval (CI): 69% to 85%]; negative predictive value, 91.3% [95% CI: 86% to 94%]) with moderate positive predictive value (50.6% [95% CI: 43% to 58%] and specificity (75.41% [95% CI: 70% to 79%]). Higher diagnostic accuracy was observed for transmural perfusion defects (sensitivity 87.8%; 95% CI: 74% to 96%) and infarcted segments (sensitivity 85.3%; 95% CI: 74% to 93%). Although eMBF in high-quality examinations was lower but not different between ischemic and infarcted segments (72.3 ± 18.7 ml/100 ml/min vs. 73.1 ± 31.9 ml/100 ml/min, respectively, $p > 0.05$), eMBV was significantly lower in infarcted segments compared with ischemic segments (11.3 ± 3.3 ml/100 ml vs. 18.4 ± 2.8 ml/100 ml, respectively; $p < 0.01$).

CONCLUSIONS Compared with CMR, dynamic stress CT provides good diagnostic accuracy for the detection of myocardial perfusion defects and may differentiate ischemic and infarcted myocardium. (J Am Coll Cardiol Img 2014;7:267–77) © 2014 by the American College of Cardiology Foundation

Given the high diagnostic accuracy of cardiac computed tomography (CT) for the morphological assessment of coronary artery stenosis, much research effort has been focused on its ability to evaluate myocardial perfusion (1). Initial studies suggest that sequential CT acquisitions of the myocardium under stress over a pre-defined period of time may allow the quantitative calculation of myocardial blood flow (MBF), which would constitute an attractive option in detecting myocardial ischemia. Studies indicate that CT-based reduced MBF values correspond to defects on radionucleotide perfusion imaging, cardiac magnetic resonance (CMR), and invasive measurement of fractional flow reserve (2–7). In clinical practice, separate acquisitions at rest and during pharmacological stress are a cornerstone of established radionuclear and CMR imaging modalities to distinguish viable from nonviable myocardium and guide treatment decisions (8). Reversible perfusion defects are regarded as viable ischemic, whereas fixed perfusion defects are interpreted as myocardial scar or necrosis.

In theory, dynamic CT perfusion imaging relies on time-attenuation curves and provides the ability to derive a set of quantitative perfusion measurements, enabling the differentiation of cellular viability within a single acquisition (9). Such algorithms have already been established for CT-based evaluation of stroke patients (10). However, although highly relevant, comparison of dynamic CT perfusion imaging with findings on established CMR has not been systematically evaluated.

We therefore studied the feasibility of sequential dynamic CT perfusion to detect and differentiate between reversible and fixed myocardial perfusion defects as defined by CMR in a cohort of subjects with known or suspected coronary artery disease. We hypothesized that CT-derived quantitative measures of perfusion may enable the differentiation of viable from nonviable myocardium.

ABBREVATIONS AND ACRONYMS

AUC = area under the curve
BW = bandwidth
CMR = cardiac magnetic resonance
CT = computed tomography
eMBF = estimated myocardial blood flow
eMBV = estimated myocardial blood volume
FA = flip angle
MBF = myocardial blood flow
MBV = myocardial blood volume
MR = magnetic resonance
NPV = negative predictive value
PPV = positive predictive value
SA = short-axis
SPECT = single-photon emission computed tomography
TE = echo time
TR = repetition time

METHODS

Study population. The study was designed as a prospective cohort study enrolling patients referred for invasive angiography due to suspected or known coronary artery disease, as described previously (2). In this substudy, enrolled subjects underwent dynamic CT-based perfusion imaging followed by adenosine-stress CMR acquisition (±1 day).

If enrolled, subjects were required to be between 50 and 80 years of age, symptomatic, and scheduled to undergo diagnostic invasive coronary angiography. Additionally, the following inclusion criteria were applied: absence of atrial fibrillation or >6 ectopic beats/min, and the ability to hold their breath for ~30 s. Exclusion criteria included clinically unstable (angina at rest, malignant arrhythmias) conditions; a history of allergy to iodinated contrast material, reactive airway disease, active hyperthyroidism, kidney disease (serum creatinine levels >1.5 mg/dl), atrioventricular block II and III, or sick sinus syndrome; pregnant or breastfeeding women; or long-term metformin treatment.

The study was approved by the Institutional Review Board of the Ludwig-Maximilians-University Munich and the Federal Radiation Safety Council (Bundesamt für Strahlenschutz), and all subjects provided written informed consent.

CT image acquisition. All CT imaging was performed on a fast dual-source CT system (Somatom Definition Flash, Siemens Healthcare, Forchheim, Germany) with 2 × 64 × 0.6 mm and flying-focal spot resulting in 2 × 128 slices under rest and stress conditions. As detailed previously, before scanning, 2 antecubital intravenous lines and electrocardiography electrodes were placed on the patient's chest, and breath holds were practiced (2).

The CT protocol included a standard prospective coronary CT angiogram (2 × 100 kVp [120 kVp in subjects with a body mass index ≥30 kg/m^2], 320 mAs/rotation, 0.28-s gantry rotation time,

From the *Department of Clinical Radiology, Ludwig-Maximilians-University, Klinikum Grosshadern, Munich, Germany; †Munich Heart Alliance, Munich, Germany; and the ‡Department of Cardiology, Ludwig-Maximilians-University, Klinikum Grosshadern, Munich, Germany. The study was supported by an unrestricted research grant by Bayer HealthCare, Berlin, Germany. The study was further supported by the DZHK (Deutsches Zentrum für Herz-Kreislauf-Forschung, German Centre for Cardiovascular Research) and the BMBF (German Ministry of Education and Research). Dr. Bamberg is on the Speakers' Bureau of Siemens Healthcare and Bayer HealthCare; and has received an unrestricted grant from Bayer HealthCare. Dr. Johnson has done research collaboration for and is on the Speakers' Bureau of Siemens Healthcare; and has received a research grant from Bayer HealthCare. All other authors have reported that they have no relationships relevant to the contents of this paper to disclose.

Manuscript received January 21, 2013; revised manuscript received May 30, 2013, accepted June 13, 2013.

0.75-mm slice thickness, end-systolically triggered at 200 ms) with iodinated contrast agent (70 ml, 5 ml/s flow [Ultravist 370, Bayer HealthCare, Berlin, Germany] followed by saline solution chaser). A test bolus of 15 ml (15 ml, 5 ml/s flow, Ultravist 370 [Bayer HealthCare]) was acquired before CT angiography as a baseline to calculate the delay for the CT angiography as well as the subsequent perfusion imaging. No beta-blockers or nitroglycerin were administered.

Dynamic CT-based perfusion imaging was performed 7 ± 2 min after baseline CT angiography, allowing for sufficient washout of the contrast media from the myocardium. Acquisition was initiated 4 s before the arrival of the contrast (50 ml at 5 ml/s, Ultravist 370 [Bayer HealthCare] followed by saline solution chaser) in the ascending aorta after, 2 min of administration of adenosine (0.14 mg/kg/min, Adrekar [adenosine], Sanofi, Munich, Germany). Scanning was continued for 30 s (both tubes, 100 kV; gantry rotation time, 0.28 s; total tube current, 300 mAs/rot) at 2 alternating table positions resulting in an effective craniocaudal imaging coverage of 73 mm. For heart rates of ≤63 beats/min, perfusion acquisition was performed for every heartbeat; for heart rates >63 beats/min, perfusion acquisition was performed for every second heartbeat (2).

CT image analysis. Image analysis was performed on an offline workstation using a commercially available dedicated software tool (MMWP, Siemens Medical Solutions, Erlangen, Germany) by 2 independent experienced observers (F.B. and K.N.) with 8 and 12 years of CT and magnetic resonance (MR) experience, respectively.

Images were reconstructed with a 3-mm slice width every 2 mm using a smooth convolution kernel (B30) and then processed on a standard workstation with commercially available perfusion software (syngo VPN, Siemens Healthcare). MBF and MBV were determined in each of the 16 myocardial segments as defined by the American College of Cardiology/American Heart Association, excluding the apical segment (11). To avoid impact by beam hardening on the measurements, a region of interest of 2.5 cm^2 was manually placed in a representative area of each myocardial segment with a 1-mm subendocardial zone directly adjacent to the contrast-filled left ventricle and a 1-mm subepicardial zone excluded from analysis (2). In case of significantly impaired image quality (due to beam hardening and or motion artifacts), the affected segment was excluded from the analysis. To estimate MBF, a dedicated parametric deconvolution technique, based on a 2-compartment model of intravascular and extravascular space, was used to fit the time attenuation curves (12). The algorithm double-sampled the arterial input function from regions of interest that were placed in the descending aorta with every table position and combined into 1 arterial input function that has twice the sampling rate of the tissue time-attenuation curve. Estimation of MBF was subsequently derived from the maximal slope of the fit model curve for every voxel, as the estimated myocardial blood volume (eMBV) was derived from the peak enhancement of the model curve (13). Overall, this approach yielded a continuous estimation of MBF and MBV per myocardial segment in ml/100 ml/min and ml/100 ml, respectively.

Evaluation of the presence of significant coronary artery stenosis (>50% luminal narrowing) and of atherosclerotic plaque was performed on axial source images in a consensus reading by 2 experienced investigators using a modified 17-segment model of the coronary artery tree (14). Readers were blinded to the subject's clinical presentation; coronary atherosclerotic plaque was visually classified as noncalcified, calcified, or mixed plaque (containing noncalcified and calcified plaque components), as detailed previously (15).

CMR. CMR was performed within 24 h after the CT scan on a 3-T whole-body MR system (Magnetom Verio, Siemens Healthcare) using a dedicated 32-element cardiac phased array coil (RAPID Biomedical GmbH, Rimpar, Germany).

Following localizer images, a small-volume shim centered on the left ventricle was applied to correct for local off-resonances in steady-state free precession images. Subsequently, cine studies in horizontal and vertical long-axis orientation were obtained for determination of the proper short-axis (SA) plane using a segmented steady-state free precession sequence (recovery time [TR] 3.0 ms; echo time [TE] 1.5 ms; flip angle (FA) 60°; bandwidth (BW) 975 Hz/pixel). MR perfusion imaging was performed using a linearly ordered saturation recovery fast spoiled gradient echo protocol (TR 2.4 ms; TE 0.86 ms; trigger delay 10 ms; BW 1002 Hz/pixel; FA 5°) in SA orientation acquiring 3 slice locations for coverage of the basal, mid, and apical part of the left ventricle. A matrix resolution of 128 × 196 at a field-of-view of 360 × 270 mm^2 rendered an in-plane resolution of 2.8 × 2.8 mm^2. Slice thickness was 10 mm.

For the late gadolinium enhancement, the entire left ventricle was covered in 2- and 4-chamber and continuous SA views from base to the apex using an inversion recovery fast spoiled gradient echo sequence (TR 5.2 ms; TE 1.98 ms; FA 20°;

BW 287 Hz/pixel), acquiring 1 slice per breath hold. Voxel size was $1.9 \times 1.4 \times 8$ mm^3. With data acquisition, every second heartbeat, imaging of 1 slice was possible in 10 cardiac cycles.

Similar to CT, hyperemia was induced with a continuous (6 min) intravenous injection of 140 μg/kg·min^{-1} adenosine (Adrekar [adenosine], Sanofi) via a venous line. A bolus of gadobutrol (Gadovist, Bayer HealthCare) of 0.05 mmol/kg body weight with a flow rate of 5 ml/s followed by 20 ml saline solution using an MR-compatible automatic injector (Spectris, Medrad, Indianola, Pennsylvania) were administered via a separate intravenous line.

CMR ANALYSIS. All acquired CMR data were transferred to an offline workstation (Dynamic Signal Analysis, Argus, Siemens Medical Solutions), with 2 blinded observers performing the analysis for each of the 16 myocardial segments. For each segment, the presence of hypoperfusion (ischemia) assessed by visual comparison of stress and rest CMR perfusion scans (subendocardial ischemia or transmural ischemia) was determined. Data were additionally evaluated for the presence of infarction (scar) on late gadolinium-enhancement images as stratified by transmurality (1% to 25%, 26% to 50%, 51% to 75%, and >75%) for each segment.

Covariates. Subject data on demographic factors and cardiovascular risk were collected prospectively. Effective radiation of each patient was derived by multiplying the dose-length-product, automatically provided by the scanner, with the conservative constant k (k = 0.017 mSv/mGy·cm).

Statistical analysis. Descriptive statistics are provided as mean ± SD or median and interquartile range for continuous variables if normally or not normally distributed, respectively. Absolute and relative frequencies are provided for categorical variables.

A paired Student *t* test was used to compare estimated myocardial blood flow (eMBF) and eMBV between normal segments and segments with ischemia and/or infarct as defined by CMR. MBF and MBV cutpoints were derived by maximization of the odds ratio in binary logistic regression modeling. The asymptotic 95% confidence intervals (CIs) for the area under the curve (AUC) were estimated using a nonparametric approach, which is closely related to the jackknife technique proposed by DeLong et al. (16).

Subsequently, we calculated conventional measures of diagnostic accuracy (sensitivity, negative predictive value [NPV], specificity, positive predictive value [PPV]), and the accuracy for any perfusion defect followed by stratified analysis for ischemic, infarcted and transmural perfusion defects. For all of these analyses, the previously derived cutpoint was used. We accounted for the clustered nature of the myocardial territories per subjects by estimating the observed distribution (95% CI) according to DeLong et al. (16).

A 2-sided p value <0.05 was considered to indicate statistical significance. All analyses were performed using SAS Version 9.1 (SAS Institute Inc., Cary, North Carolina).

RESULTS

Over the study period, 127 patients met the inclusion criteria, of whom 51 were deemed protocol eligible (Fig. 1). Ten subjects refused participation in the general study, 5 subjects refused the optional MR examination, and in 5 subjects, the study interfered with clinical care. Among enrolled subjects, the imaging protocol was aborted due to technical failure of the CT scanner in 3 subjects, and in 4 subjects, the MR examination was incomplete (claustrophobia in 4 subjects). Not all subjects subsequently underwent invasive coronary angiography. Thus, 31 subjects completed the study protocol and were included in the analysis. Overall, these were predominantly middle-aged men with a high prevalence of a history of coronary artery disease and multiple cardiovascular risk factors; details are provided in Table 1. CT coronary angiographic findings for all subjects are provided in Table 2. Among these subjects, 484 myocardial segments were included in the analysis (12 segments were excluded due to incomplete coverage and/or severely impaired image quality).

The average acquisition time of the dynamic CT-based perfusion protocol was 6.32 ± 17.4 min with an effective average radiation exposure of 16.91 ± 3.25 mSv (5.83 ± 2.85 mSv and 11.08 ± 2.07 mSv for the CT angiography and the perfusion acquisition, respectively). Representative images of normal, ischemic, and infarcted myocardium are provided in Figures 2 to 4; derived tissue-attenuation curves are shown in Figure 5. The mean heart rate under rest and stress conditions was 69 beats/min and 88 beats/min, respectively. On average, the eMBF for all myocardial segments was 103.1 ± 37.1 ml/100 ml/min, whereas the mean eMBV was 17.7 ± 5.4 ml/100 ml. Intraobserver and interobserver agreement for eMBF and eMBV was high (intraclass coefficient: 0.81 and 0.80, respectively). The average acquisition time of the CMR perfusion protocol was 41 ± 8 min, and the heart rate

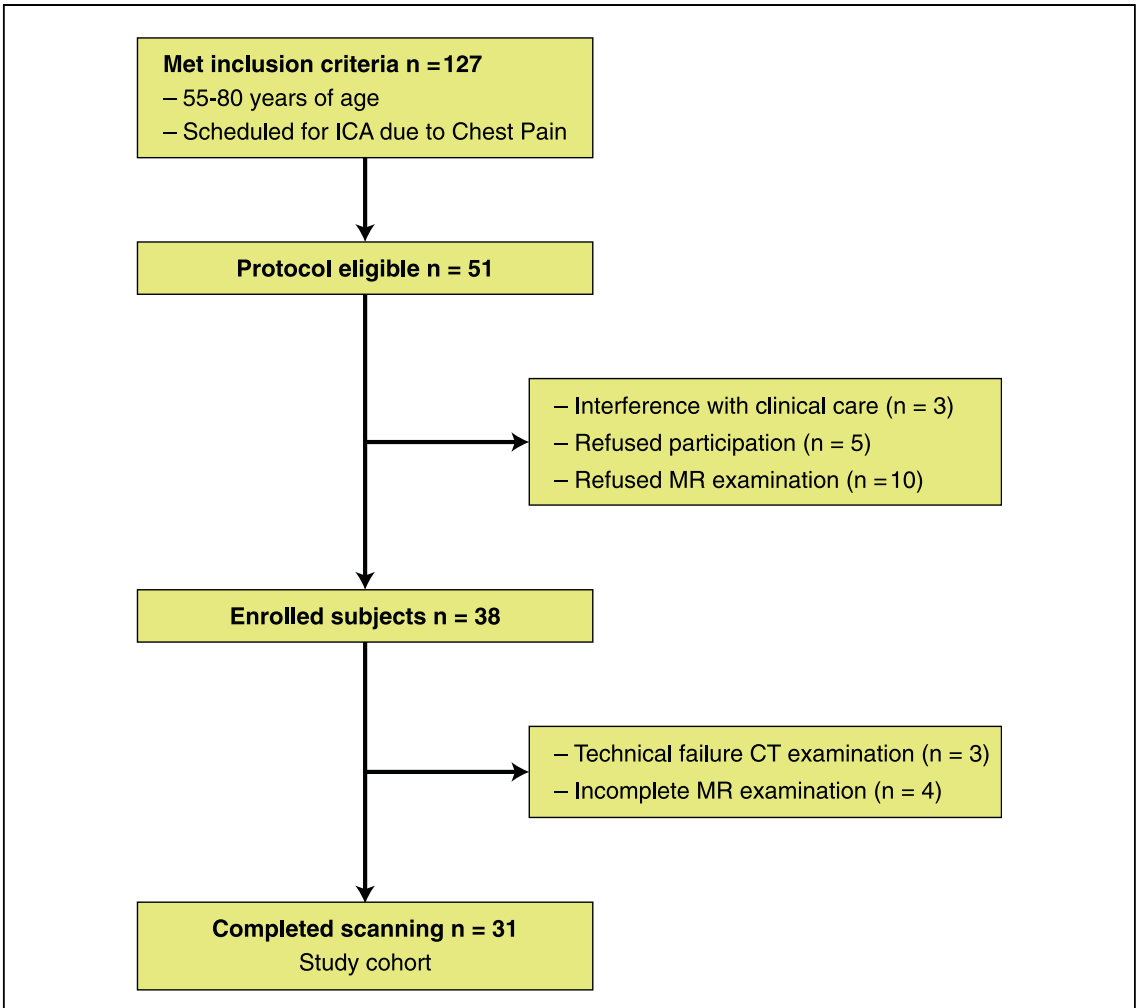

Figure 1. Study Flow Chart

CT = computed tomography; ICA = invasive coronary angiography; MR = magnetic resonance.

similarly increased from rest to stress conditions (65 ± 13 beats/min to 90 ± 17 beats/min, respectively).

Table 1. Demographic and Cardiovascular Risk Factors of the Study Cohort

Age, yrs	70.4 ± 9.3
Male	74.0
Hypertension	86.7
Diabetes mellitus	20.0
Current smoking	26.7
Hyperlipidemia	43.3
History of coronary artery disease	86.7
History of stent placement	58.6
Body mass index, kg/m^2	26.56 ± 4.12

Values are mean ± SD or %.

The prevalence of a perfusion defect by CMR as the established gold standard was high (24.2%). Of these, 56 were classified as ischemic (11.6%), and 61 were classified as infarcted (12.6%). Approximately two-thirds (8.5%, n = 41) of infarcted segments were categorized with transmural extent. The presence and extent of coronary artery disease by CT angiography were significantly higher among patients with a perfusion defect on CMR compared with subjects without perfusion defects on CMR (Table 2). Myocardial segments with perfusion defects on CMR had significantly lower CT-based eMBF and eMBV values compared with segments without perfusion defects on CMR (eMBF 72.72 ± 25.76 ml/100 ml/min vs. 112.73 ± 35.06 ml/100 ml/min and MBV 15.4 ± 6.09 ml/100 ml vs. 18.45 ± 5.00 ml/100 ml for myocardial segments with perfusion defects vs. no perfusion defect on CMR,

Table 2. Presence of Coronary Atherosclerotic Plaques and Stenosis as Determined by CT Coronary Angiography

	All	With MR Perfusion Defects	Without MR Perfusion Defects	p Value
No.	31	23 (74.2)	8 (25.8)	
Any plaque	30 (96.8)	23 (100.0)	7 (87.5)	0.08
Any stenosis	27 (87.1)	22 (95.6)	5 (62.5)	0.01

Values are n or n (%).
CT = computed tomography; MR = magnetic resonance.

respectively). Maximizing the AUC, receiver-operating characteristic analysis revealed a cutpoint of 88 ml/100 ml/min and 16 ml/100 ml, respectively, to provide the highest differentiation between segments with and without perfusion defects on CMR, which was applied for all subsequent analyses. As such, the prevalence of myocardial segments with hypoperfused segments on CT was 37.1% and 16.0% for eMBF and eMBV, respectively.

Conventional measures of diagnostic accuracy are provided in Tables 3 and 4. Overall, the diagnostic accuracy of CT perfusion for the detection of any perfusion defect as determined by CMR on a per-segment basis was good (sensitivity 77.8% [95% CI: 69% to 85%]; NPV 91.3% [95% CI: 88% to 94%]). On a per-vessel and per-patient basis, all of the present perfusion defects were correctly identified (22 of 22 and 23 of 23, respectively), resulting in a sensitivity and NPV of 100%. The associated PPV was moderate at 50.6% (95% CI: 43% to 58%) but higher on a per-vessel and per-patient basis (PPV 92.0% [95% CI: 73% to 99% and 92.0% [95% CI: 74% to 99%]), respectively).

When stratified by ischemic and infarcted segments, the diagnostic accuracy for the detection of infarcted segments was higher than for ischemic segments (sensitivity 85.3% [95% CI: 74% to 93%] vs. 69.6% [95% CI: 56% to 81%]). The corresponding NPV was similarly higher for infarcted compared with ischemic myocardial segments (NPV 95.0% [95% CI: 91% to 98%] and 91.0% [95% CI: 86% to 95%]). In contrast, the diagnostic accuracy for the detection of any transmural perfusion defect was excellent (sensitivity 87.80% [95% CI: 74% to 96%] and NPV 97.2% [95% CI: 94% to 99%]).

In a subgroup of 17 patients with excellent image quality on CT, the measured eMBF was similar in infarcted and ischemic myocardial segments (eMBF 73.1 ± 31.9 ml/100 ml/min vs. 72.3 ± 18.7 ml/100 ml/min, respectively; p = 0.68) (Fig. 6). In contrast, eMBV was significantly lower in infarcted segments compared with ischemic myocardial segments (eMBV 11.33 ± 3.29 ml/100 ml vs. 18.37 ± 2.77 ml/100 ml for infarcted vs. ischemic myocardial segments, respectively) (Fig. 6).

DISCUSSION

In the present study, we investigated the feasibility of dynamic, sequential myocardial CT perfusion imaging to detect and characterize perfusion defects compared with CMR as the gold standard. Our results indicate that dynamic CT perfusion imaging has the highest diagnostic accuracy in detecting (transmural) infarcted myocardial segments and good diagnostic accuracy in detecting any other perfusion defects, when relying solely on eMBF. Although infarcted segments did not differ from reversible ischemic segments with respect to eMBF, eMBV as another quantitative measurement may help in differentiating viable from nonviable myocardium.

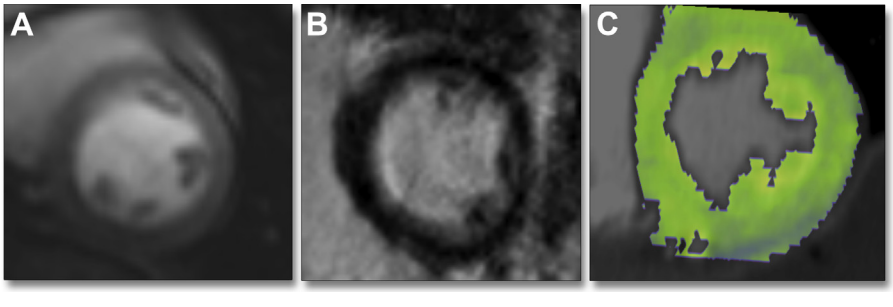

Figure 2. A 62-Year-Old Man With Typical Angina Scheduled for Invasive Angiography

Stress-perfusion magnetic resonance (MR) shows regular mid-ventricular enhancement **(A)** and the absence of late gadolinium enhancement in the delayed MR imaging sequences **(B)**. Corresponding dynamic computed tomography perfusion imaging reconstruction of the myocardium with derived myocardial blood flow and volume of 142.00 ml/100 ml/min and 17.47 ml/100 ml, respectively **(C)**.

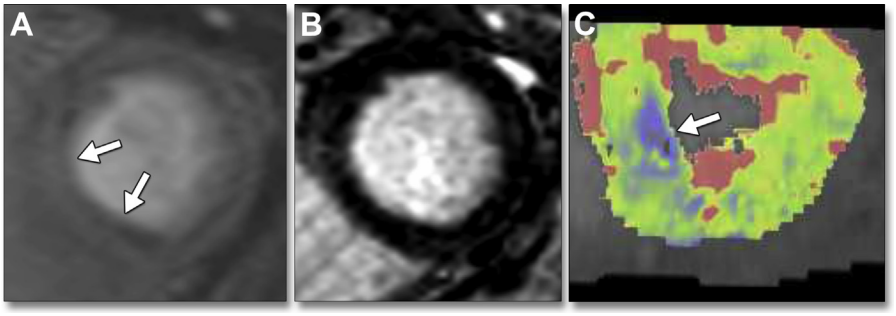

Figure 3. A 58-Year-Old Woman With Atypical Angina Referred for Invasive Angiography

Stress perfusion cardiac magnetic resonance reveals a mid-ventricular inferoseptal subendocardial perfusion defect **(A, arrows)** and absence of late gadolinium enhancement in the delayed sequences **(B)**. Dynamic computed tomography perfusion imaging **(C)** indicates a color-coded perfusion defect **(blue)** in the inferoseptal wall (myocardial blood flow 60.42 ml/100 ml/min; myocardial blood volume, 17.00 ml/100 ml) **(arrow)**.

Our results provide initial evidence that dynamic myocardial CT perfusion imaging provides high sensitivity and NPV for perfusion defects, a finding that is consistent when looking at vessel territories and subjects (100% sensitivity and NPV on a per-segment and per-patient basis, respectively) but lower PPV. Partially, this finding can certainly be attributed to the high pretest likelihood of disease (24% prevalence of perfusion defects), but may also indicate some of the limitations and artifacts of the current dynamic perfusion CT technique. In fact, partial volume, motion, and breathing artifacts may show false lowered eMBF values and may in part explain the generally observed lower specificity and PPV. One should also take into consideration that the computation is based on a nonphysiological simplified assumptive compartment model. A new distribution technique, which takes the temporal and spatial gradients in uptake and retention along the capillary into consideration, might provide better results (17). This indicates the necessity for further improvements of the underlying algorithms to widen the applicability on a wide range of patients.

These findings are consistent with and extend those from previous reports on the technique's diagnostic accuracy, including single-photon emission computed tomography (SPECT) and CMR (4,6,7,18,19). In 1 study (n = 35), Ho et al. (6) found similarly high sensitivity and NPV for the detection of myocardial perfusion defects (83% sensitivity, 82% NPV). Thus, we confirm these initial findings but provide a relevant subgroup analysis to elucidate the ability to differentiate reversible from fixed perfusion defects. In contrast

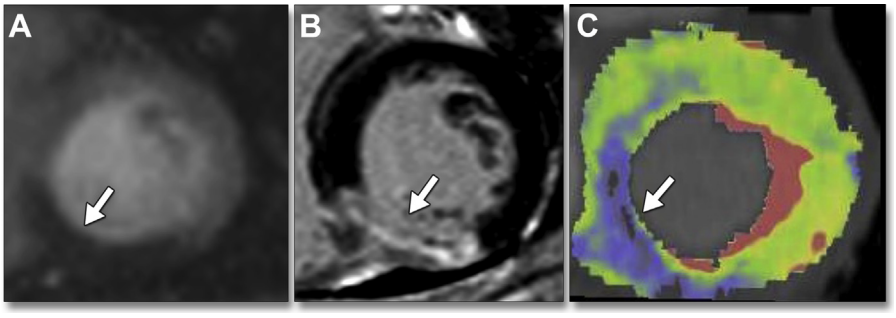

Figure 4. A 56-Year Old Man With a Known History of Myocardial Infarction

(A) Stress perfusion cardiac magnetic resonance demonstrates a transmural perfusion defect in the posterior wall **(arrow)** that corresponds to pathological enhancement in the late gadolinium sequences indicating myocardial scar **(B, arrow)**. The dynamic stress perfusion imaging by computed tomography **(C)** indicates decreased perfusion in the inferior wall (myocardial blood flow 46 ml/100 ml/min; myocardial blood volume 15 ml/100 ml) **(arrow)**.

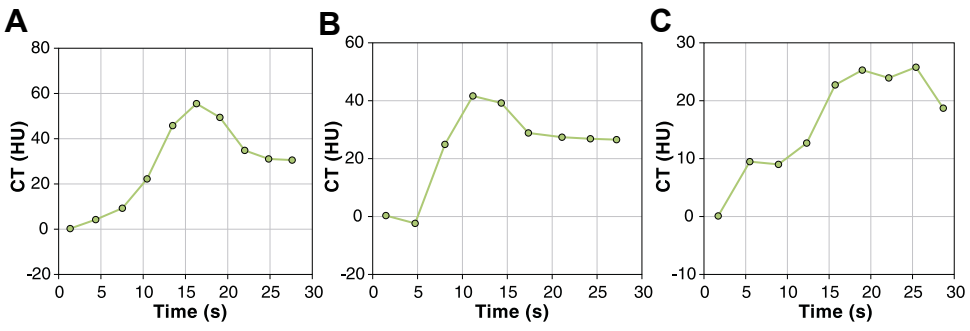

Figure 5. Tissue Attenuation Curves Obtained From Dynamic CT Perfusion Imaging

Normal myocardium **(A)**, ischemic myocardium **(B)**, infarcted myocardium **(C)**. CT = computed tomography; HU = Hounsfield units.

to our results, a previous initial study applying CMR as the gold standard showed a higher specificity than sensitivity for the detection of perfusion defects (86% sensitivity vs. 98% specificity) (19). However, these findings were based on 10 subjects, and the prevalence of perfusion defects was very high (60% prevalence).

In contrast to previous work, we determined differences between viable and nonviable myocardium and found that although infarcted segments are generally detected with a high diagnostic accuracy (85.3% sensitivity), the diagnostic accuracy for the detection of ischemic myocardium is lower (69.6% sensitivity), although the NPV was maintained. Interestingly, this corresponds to previous experimental sequential CT imaging research using a different CT setup. George et al. (4) reported a sensitivity of 72% when comparing those findings with SPECT data. Our sensitivity was similar, but we found a lower specificity than in their previous report (91%). This observation can be mainly attributed to the fact that we prospectively excluded an area of 1 mm from the subendocardial border to avoid any beam hardening effects, and most reversible perfusion defects were subendocardial. This effect is emphasized by the finding that for the detection of transmural perfusion defects, sensitivity increases to 87.8% (36 of 41 segments detected). Because perfusion defects are generally most pronounced in the subendocardium, further work will be necessary to reduce beam hardening in the myocardial border. Due to its high spatial resolution, there is emerging evidence that CMR has the highest potential to detect and characterize subendocardial perfusion defects and may be superior to SPECT (20).

One interesting finding in our study is that eMBV is reduced in infarcted segments compared with ischemic segments and restricted to high-quality acquisitions. eMBV is defined as the peak enhancement, which is calculated by dividing the maximum point of the time-attenuation curve by the maximum point of the arterial input function (13). This can be explained by the low capillary density in fibrotic tissue compared with normal myocardium, which results in a lower peak enhancement. In fact, this is also in line with the observation of late contrast enhancement observed

Table 3. Diagnostic Accuracy of Dynamic CT-Based Perfusion Imaging for the Detection of Any Ischemia and/or Infarction on Cardiac MR Stratified by Myocardial Segment, Per Vessel, and Per Subject

	Sensitivity	Specificity	PPV	NPV	Accuracy
Per segment	77.8 (91/117)	75.4 (273/362)	50.6 (91/180)	91.3 (273/299)	76.0 (364/479)
MBF positive	69.2–84.9	70.6–79.8	43.0–58.1	87.5–94.2	0.71–0.80
Per vessel territory	100.0 (23/23)	75.0 (6/8)	92.0 (23/25)	100.0 (6/6)	93.5 (29/31)
MBF positive	84.6–100.0	34.9–96.8	73–99.0	54.1–100.0	78.5–99.2
Per subject	100.0 (23/23)	75.0 (6/8)	92.0 (23/25)	100.0 (6/6)	93.5 (29/31)
MBF positive	85.2–100	34.9–96.8	74.0–99.0	54.1–100.0	78.5–99.2

Values are % (n/N) and 95% confidence interval. Numbers in parentheses indicate number of segments, vessels, and subjects, respectively.
MBF = myocardial blood flow; NPV = negative predictive value; PPV = positive predictive value; other abbreviations as in Table 2.

Table 4. Diagnostic Accuracy of Dynamic CT-Based Perfusion Imaging for the Detection of Ischemic and Infarcted Myocardium and Any Subendocardial Perfusion Defects Compared With Cardiac MR

	Sensitivity	Specificity	PPV	NPV	Accuracy
Infarcted myocardium					
Per segment	85.3 (52/61)	70.5 (172/244)	41.9 (52/124)	95.0 (172/181)	73.4 (224/305)
MBF positive	73.8–93.0	64.3–76.1	33.1–51.1	90.8–97.7	68.1–78.3
Ischemic myocardium					
Per segment	69.6 (39/56)	70.5 (172/244)	35.1 (39/111)	91.0 (172/189)	70.3 (211/300)
MBF positive	55.9–81.2	64.3–76.1	26.3–44.8	86.0–94.7	64.8–75.5
Transmural perfusion defects					
Per segment	87.8 (36/41)	70.49 (172/244)	33.3 (36/108)	97.2 (172/177)	73.0 (208/285)
MBF positive	73.8–95.9	64.34–76.14	24.6–43.1	93.6–99.1	67.4–78.1

Values are % (n/N) and 95% confidence interval. Numbers in parentheses indicate number of segments, vessels, and subjects, respectively. Abbreviations as in Tables 2 and 3.

on CT and CMR, indicating the replacement of normal myocytes by scar tissue (21).

In this study, we applied a threshold of 88 ml/100 ml/min for eMBF to indicate a perfusion defect. This is in contrast to a previously published threshold by our group (75 ml/100 ml/min) in a feasibility study, with fractional flow reserve serving as standard of reference (2). This derivation was due to an optimization of the AUC (0.84 vs. 0.78 when applying the fractional flow reserve reference). The application of a standardized threshold should be used with care. In our study, 1 patient had a globally low eMBF, but showed neither ischemic nor infarcted areas on CMR. Previous work in this area indicates that the interpretation of eMBF varies. Studies by Ho et al. (6) and Nakauchi et al. (18) were more descriptive, by not using a threshold but rather by comparing qualitatively the hypoperfused area with surrounding normally perfused myocardium. Although this approach may be applied on significant hypoperfused myocardium, it may be challenging for less significant areas. Also, we performed

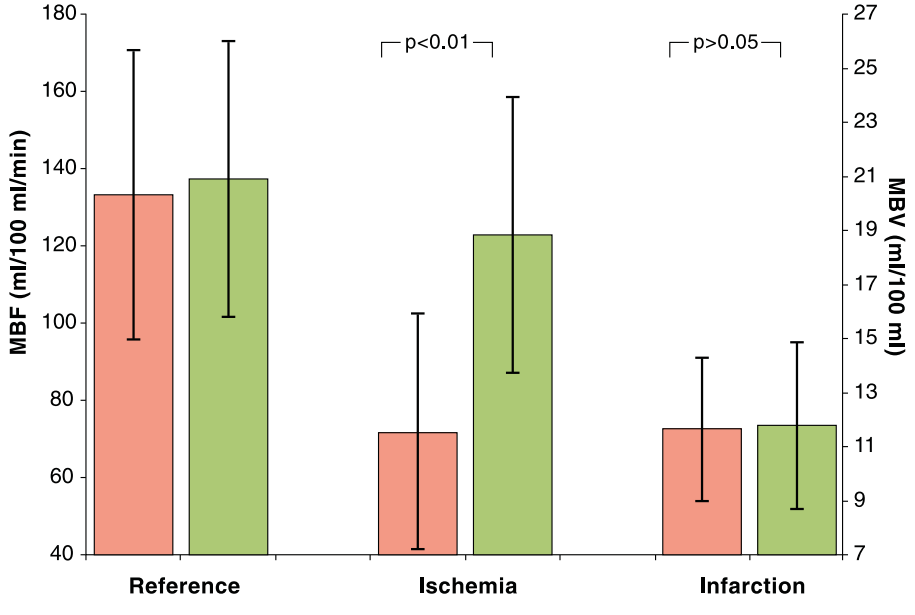

Figure 6. Bar Diagram for Differences in MBF and MBV

Differences in myocardial blood flow (MBF) **(pink)** and myocardial blood volume (MBV) **(green)** between reference myocardium as well as ischemic and infarcted myocardium in 17 subjects with excellent image quality.

CT angiography before the CT perfusion imaging, which may have affected the observed perfusion values. This proves that further research is required to establish valid reference values in larger cohorts (i.e., multicenter studies) in order to be applied in a potential clinical setting.

Study limitations. There are a number of aspects that limit the wide clinical use of the technique. The effective radiation dose was high (mean 11.08 ± 2.07 mSv); thus, further developments with respect to radiation dose savings are necessary. Also, the width of the detector (and the imaging volume) was relatively low (73 mm), providing insufficient coverage of the myocardium in a number of cases. In addition, the breath-hold and scan duration of 30 s remained challenging for the majority of participants.

An alternative to the dynamic acquisition of the myocardium is the single-shot acquisition for the assessment of myocardial perfusion, which is associated with substantially lower radiation exposure (up to 2.5 ± 2.1 mSv when using high-pitch protocols) and comparable diagnostic accuracy (78% sensitivity and 84% NPV) (22). However, similar to the assessment of delayed enhancement in CT, single-shot acquisition protocols are limited to a merely qualitative image evaluation whereas, per se, the dynamic approach is more objective, based on a numerical evaluation. Further, comparative studies are warranted to compare both approaches of CT-based myocardial perfusion imaging.

The results of our study need to be evaluated in the context of its limitations. There may be a substantial source of selection bias present, as only a fraction of eligible subjects finally were enrolled in the study. This was primarily due to the complexity of the study protocol but also to contraindications to the administration of adenosine. Thus, the results may only apply to a very restricted population. However, restriction to the use of adenosine and complexity of the imaging protocol are also an inherent limitation of other functional imaging modalities such as CMR. In fact, the duration of the CT perfusion examination was slightly shorter, but restricted to 1 stress acquisition only.

Finally, we applied CMR as the gold standard; thus, our findings may have been different when applying, for example, SPECT, as the standard of reference.

CONCLUSIONS

Our study indicates that dynamic CT perfusion imaging provides good diagnostic accuracy for the detection of myocardial perfusion defects compared with CMR. Although the ability of CT perfusion imaging to detect infarcted segments was generally higher than for ischemic segments, an eMBV may help to differentiate viable from nonviable myocardium in 1 single CT stress acquisition.

Acknowledgments

The authors acknowledge the support of the CT technologists and staff at the Department of Clinical Radiology of the Ludwig-Maximilian-University, Klinikum Grosshadern, Munich, Germany.

Reprint requests and correspondence: Dr. Fabian Bamberg, Department of Clinical Radiology, Ludwig-Maximilians-University, Marchioninistrasse 15, 81377 Munich, Germany. *E-mail: fbamberg@med.lmu.de.*

REFERENCES

1. Cerci RJ, Arbab-Zadeh A, George RT, et al. Aligning coronary anatomy and myocardial perfusion territories: an algorithm for the CORE320 Multicenter Study. Circ Cardiovasc Imaging 2012;5:587–95.
2. Bamberg F, Becker A, Schwarz F, et al. Detection of hemodynamically significant coronary artery stenosis: incremental diagnostic value of dynamic CT-based myocardial perfusion imaging. Radiology 2011;260:689–98.
3. So A, Hsieh J, Imai Y, et al. Prospectively ECG-triggered rapid kV-switching dual-energy CT for quantitative imaging of myocardial perfusion. J Am Coll Cardiol Img 2012;5:829–36.
4. George RT, Arbab-Zadeh A, Miller JM, et al. Computed tomography myocardial perfusion imaging with 320-row detector computed tomography accurately detects myocardial ischemia in patients with obstructive coronary artery disease. Circ Cardiovasc Imaging 2012;5:333–40.
5. Bastarrika G, Ramos-Duran L, Rosenblum MA, Kang DK, Rowe GW, Schoepf UJ. Adenosine-stress dynamic myocardial CT perfusion imaging: initial clinical experience. Invest Radiol 2010;45:306–13.
6. Ho KT, Chua KC, Klotz E, Panknin C. Stress and rest dynamic myocardial perfusion imaging by evaluation of complete time-attenuation curves with dual-source CT. J Am Coll Cardiol Img 2010;3:811–20.
7. Wang Y, Qin L, Shi X, et al. Adenosine-stress dynamic myocardial perfusion imaging with second-generation dual-source CT: comparison with conventional catheter coronary angiography and SPECT nuclear myocardial perfusion imaging. AJR Am J Roentgenol 2012;198:521–9.
8. Hendel RC, Patel MR, Kramer CM, et al. ACCF/ACR/SCCT/SCMR/ASNC/NASCI/SCAI/SIR 2006 appropriateness criteria for cardiac computed tomography and cardiac magnetic resonance imaging: a report of the American College of Cardiology Foundation Quality Strategic Directions

Committee Appropriateness Criteria Working Group, American College of Radiology, Society of Cardiovascular Computed Tomography, Society for Cardiovascular Magnetic Resonance, American Society of Nuclear Cardiology, North American Society for Cardiac Imaging, Society for Cardiovascular Angiography and Interventions, and Society of Interventional Radiology. J Am Coll Cardiol 2006;48:1475–97.

9. Bamberg F, Klotz E, Flohr T, et al. Dynamic myocardial stress perfusion imaging using fast dual-source CT with alternating table positions: initial experience. Eur Radiol 2010;20:1168–73.
10. Wechsler LR. Imaging evaluation of acute ischemic stroke. Stroke 2011;42:S12–5.
11. Cerqueira MD, Weissman NJ, Dilsizian V, et al. Standardized myocardial segmentation and nomenclature for tomographic imaging of the heart: a statement for healthcare professionals from the Cardiac Imaging Committee of the Council on Clinical Cardiology of the American Heart Association. Circulation 2002;105:539–42.
12. Bruder H, Raupach R, Klotz E, Stierstorfer K, Flohr T. Spatio-temporal filtration of dynamic CT data using diffusion filters. Medical Imaging 2009: Physics of Medical Imaging. SPIE, Lake Buena Vista, FL: 2009:725857–10.
13. Mahnken AH, Klotz E, Pietsch H, et al. Quantitative whole heart stress perfusion CT imaging as noninvasive assessment of hemodynamics in coronary artery stenosis: preliminary animal experience. Invest Radiol 2010;45:298–305.
14. Austen WG, Edwards JE, Frye RL, et al. A reporting system on patients evaluated for coronary artery disease. Report of the Ad Hoc Committee for Grading of Coronary Artery Disease, Council on Cardiovascular Surgery, American Heart Association. Circulation 1975;51:5–40.
15. Bamberg F, Dannemann N, Shapiro MD, et al. Association between cardiovascular risk profiles and the presence and extent of different types of coronary atherosclerotic plaque as detected by multidetector computed tomography. Arterioscler Thromb Vasc Biol 2008;28:568–74.
16. DeLong ER, DeLong DM, Clarke-Pearson DL. Comparing the areas under two or more correlated receiver operating characteristic curves: a nonparametric approach. Biometrics 1988;44:837–45.
17. Alessio AM, Bassingthwaighte JB, Glenny R, Caldwell JH. Validation of an axially distributed model for quantification of myocardial blood flow using ^{13}N-ammonia PET. J Nucl Cardiol 2013;20:64–75.
18. Nakauchi Y, Iwanaga Y, Ikuta S, et al. Quantitative myocardial perfusion analysis using multi-row detector CT in acute myocardial infarction. Heart 2012;98:566–72.
19. Weininger M, Schoepf UJ, Ramachandra A, et al. Adenosine-stress dynamic real-time myocardial perfusion CT and adenosine-stress first-pass dual-energy myocardial perfusion CT for the assessment of acute chest pain: initial results. Eur J Radiol 2012;81:3703–10.
20. Wagner A, Mahrholdt H, Holly TA, et al. Contrast-enhanced MRI and routine single photon emission computed tomography (SPECT) perfusion imaging for detection of subendocardial myocardial infarcts: an imaging study. Lancet 2003;361:374–9.
21. Arai AE. The cardiac magnetic resonance (CMR) approach to assessing myocardial viability. J Nucl Cardiol 2011;18:1095–102.
22. Feuchtner G, Goetti R, Plass A, et al. Adenosine stress high-pitch 128-slice dual-source myocardial computed tomography perfusion for imaging of reversible myocardial ischemia: comparison with magnetic resonance imaging. Circ Cardiovasc Imaging 2011;4:540–9.

Key Words: cardiac CT ■ cardiac MR ■ infarct ■ ischemia ■ myocardial perfusion.